Biophysical Journal Volume 75 December 1998 3135–3142

X-Ray Absorption Fine-Structure Spectroscopy Studies of Fe Sites in Natural Human Neuromelanin and Synthetic Analogues

A. J. Kropf,* B. A. Bunker,* M. Eisner,# S. C. Moss,# L. Zecca,§ A. Stroppolo,§ and P. R. Crippa¶

*Department of Physics, University of Notre Dame, Notre Dame, Indiana 46556 USA, #Department of Physics, University of Houston, Houston, Texas 77204-5506 USA, §Institute of Advanced Biomedical Technologies—CNR, Via Ampere 56, 20131 Milan, Italy, and ¶Department of Environmental Science, University of Parma and INFM, Parma, Italy

ABSTRACT X-ray absorption fine-structure spectroscopy is used to study the local environment of the iron site in natural (human) neuromelanin extracted from substantia nigra tissue and in various synthetic neuromelanins. All the materials show Fe centered in a nearest neighbor sixfold (distorted) oxygen octahedron; the Fe-O distances, while slightly different in the natural and synthetic neuromelanin, are both ~2.0 Å. Appreciable differences arise, however, in the second (and higher) coordination shells. In this case the synthetic melanin has the four planar oxygens bound to carbon rings with Fe-C distances of ~2.82 and 4.13 Å; the human sample does not show the 2.82 Å link but instead indicates a double shell at approximately 3.45 and 3.78 Å.

INTRODUCTION

Neuromelanin (NM) is a form of melanin found in the brain particularly in the substantia nigra (SN) and locus ceruleus. Several hypotheses have been proposed concerning the toxic or protective role of NM with respect to degeneration of dopaminergic neurons of SN (Swartz et al., 1992). In normal subjects NM accumulates with age, reaching a maximum between ages 60 and 70, while in patients afflicted with Parkinson's disease a loss of highly pigmented dopamine neurons is observed (Hirsch et al., 1988; Gibb, 1992). Along with this loss of NM, an increase in Fe, which is preponderantly bound to NM, is observed (Jellinger et al., 1992). The behavior of NM is similar to that of other melanins in that it binds metals and drugs strongly and has a characteristic electron spin resonance signal; however, the method of formation of NM in the brain appears to be different from the formation of melanin in the skin in that there are no melanocytes present and the precursor is dopamine rather than tyrosine. The concentration of iron in SN and its NM has been studied with different methods (Zecca et al., 1994, 1996) and the nature of the Fe-NM complex remains of particular interest. The small amount of SN sample available and the difficulty of extracting and purifying the NM from the SN along with the possible alterations of the material during preparation and purification has led to attempts to generate a synthetic analogue for NM. The methods for preparing synthetic analogues as well as the need for purification of samples of human NM are discussed below.

Following the discovery of the increased concentration of iron in the SN of Parkinson patients, several studies have been devoted to the interaction between Fe ions and NM. The aim of these studies was the identification of the Fe binding site(s) in order to clarify the possible role of such an interaction in the free radical production that leads to the observed degeneration of pigmented neurons. A first Mössbauer experiment, performed on synthetic dopamine melanin containing ^{57}Fe(3+) (Bardani et al., 1982), showed a superparamagnetic behavior attributed to the presence of very small particles identified with the "protomolecular" units formed by the stacking of 4–8 planar melanin monomers (Cheng et al., 1994). IR spectra suggested that the binding site is provided mainly by the *o*-phenolic functionalities (Bardani et al., 1982). A more recent Mössbauer study of purified human SN NM (Gerlach et al., 1995) has again been interpreted to indicate the presence of superparamagnetism, but with rather different Mössbauer parameters, similar to those found for hemosiderin and ferritin, the iron-storage proteins. In addition, this study has shown the presence of Fe(3+) only, in a concentration about three times higher than previously determined by x-ray fluorescence (2.8 ± 1.4 vs. 0.92%). However the determination of iron content by Mössbauer spectroscopy is not accurate. In the same work it is concluded that the iron in NM is in a form similar to that found in hemosiderin. This conclusion is in conflict with a model for Fe-NM involving two binding sites having different affinities based on a Scatchard analysis of the equilibrium saturation of ^{59}Fe(3+) bound to synthetic dopamine melanin (Ben-Shachar and Youdim, 1993). From these brief considerations, we see that natural human brain NM and the synthetic analogues seem to be structurally different and more studies are necessary in order to characterize better the nature of the Fe-NM complex. In this work we use x-ray absorption fine-structure spectroscopy (XAFS) techniques to examine the near neighborhood structure of iron in both synthetic and natural NM samples in which the metal binding sites have been saturated with iron. In order to clarify the question of whether there is more than one iron binding site we also examine a

Received for publication 22 August 1998 and in final form 9 September 1998.

Address reprint requests to Dr. Melvin Eisner, Physics Department, University of Houston, Houston, TX 77204-5506. Tel.: 713-743-3557; Fax: 713-743-3589; E-mail: eisner@shasta.phy.uh.edu.

0006-3495/98/12/3135/08 $2.00

natural NM sample in which the more easily depletable iron has been removed, as discussed in the following section.

Finally, a sample of synthetic L-dopa melanin saturated with iron was also examined in order to determine whether there is a difference in the structure of the iron melanin complex in different melanins.

MATERIALS AND METHODS

Sample preparation

Isolation of neuromelanin from human substantia nigra

Pooled samples of a SN (from 25 patients) were weighed and put into 30-ml glass centrifuge tubes with each tube containing 0.5 g of SN tissue. After homogenization with a Teflon pestle, 15 ml of water were introduced into each tube and the tissue was suspended with shaking. The tubes were then centrifuged at 10,000 rpm for 10 min at 10°C. After discarding the supernatant, the resulting pellets were washed twice with 15 ml of phosphate buffer (0.05 M, pH 7.4). To remove the proteic component the sample was incubated at 37°C for 3 h with 10 ml of Tris buffer solution (0.050 M, pH 7.5) containing sodium dodecyl sulfate (5 mg/ml). At the end of the incubation period, the suspension was centrifuged at 10,000 rpm for 20 min at 20°C and, after removing the supernatant, an aliquot of 10 ml of the previously described incubating solution, with the addition of 0.2 mg/ml of proteinase K, was added. The sample was incubated again for 3 h at 37°C. The pigment was separated by centrifugation as above and the content of the individual sample tubes were combined into a single tube and washed twice with 5 ml of NaCl solution (9 mg/ml). The sample was divided into two parts: one part was reserved to serve as the saturated (undepleted) iron NM sample while the other was treated to remove part of the iron to form the depleted sample. In order to remove the iron, the sample was incubated with 3 ml of 0.15 M EDTA-Na_2, pH 7.4, for 7 h and shaken in the dark while at room temperature. Subsequent to incubation the suspension was centrifuged at 10,000 rpm for 30 min at 20°C and then washed with 5 ml of water.

The saturated (undepleted) and depleted iron samples were both further purified as follows. To remove salts and other low molecular weight substances, the pigment was suspended in 2 ml of bidistilled water and placed into dialysis tubing with molecular weight cutoff at 12,000–14,000 (Spectrum Medical Industries, Inc., Los Angeles, CA) which had previously been treated with the same EDTA solution as above to remove any residual iron. The dialysis tube was introduced into 2,000 ml of bidistilled water and the dialysis carried out with gentle stirring at room temperature. The water in the bath was replaced every 7 h and the dialysis continued for 48 h. Following dialysis the sample was transferred into a 3-ml glass tube and centrifuged (5000 rpm, 30 min at 20°C). After discarding the supernatant the sample was resuspended in 1 ml of methanol, sonicated for 5 min, and centrifuged (5000 rpm, 30 min at 20°C) and the supernatant discarded. The precipitate was resuspended with 1 ml of hexane, again centrifuged as above, and the resulting NM sample was then dried under vacuum and weighed, yielding about 4.2 mg of iron-saturated (undepleted) NM and 3.9 mg of iron-depleted NM. The content of iron was measured by total reflection x-ray fluorescence as previously reported (Zecca et al., 1996) and was 9.8 μg/mg in the iron-saturated (undepleted) NM and 4.3 μg/mg in the iron-depleted NM.

The procedure here employed for preparation of natural NM samples has been extensively reported and discussed in our previous work (Zecca et al., 1992, 1996; Shima et al., 1997). This is a mild procedure which does not use the acid and high temperature treatments used in other studies. This insures the stability of the sample and the reproducibility of parameters such as elemental analysis, metal content, IR spectrum, electron spin resonance spectrum, pyrolysis gas chromatography-mass spectrometry spectra and chemical degradation products. The same control methods have been used for the synthetic NM samples. As previously reported (Shima et al., 1997; Zecca et al., 1996) NM seems to play a protective role in SN neurons because of its strong chelating ability which protects the neurons from iron and other metal toxicities.

The particular structure, and the differences in chelating groups, of the basic NM molecule compared to synthetic analogues are studied in this paper. We present below evidence that the structure, biosynthesis, and precursors of NM are different from those traditionally proposed. An investigation of the structure of NM-Fe complex isolated from Parkinson's disease patients would be additionally interesting to evaluate eventual changes caused by the increased peroxidation present in Parkinson's disease.

Preparation of synthetic neuromelanins

Samples of synthetic NMs were prepared both with auto-oxidative and enzymatic procedures. The aim was to match the synthetic product as closely as possible with the natural NM with regard to sulfur content, precursors, and conditions of melanization.

Enzymatic procedure

150 mg of dopamine and 19.8 mg of cysteine were dissolved in a flask containing 98 ml of 0.05 M sodium phosphate buffer (pH 7.4) and 19.6 mg of tyrosinase (EC 1.14.18.1, Sigma, St. Louis, MO) was added. The molar ratio of dopamine to cysteine in this solution is 6:1. The solution was allowed to react under O_2/CO_2 flow at room temperature for 48 h, and the reaction was then stopped by decreasing the pH to 3.0 with 30% acetic acid. The suspension was transferred into glass tubes and centrifuged at 10,000 rpm for 10 min at 25°C. The precipitate was suspended in 20 ml of 0.050 M Tris buffer (pH 7.4) containing 5 mg/ml of sodium dodecyl sulfate and allowed to incubate at 37°C for 2 h; it was then washed with 10 ml of NaCl (9 mg/ml) and centrifuged. In order to remove all trace metals, the melanin was reacted with 40 ml of 0.15 M EDTA-Na_2 for 8 h and centrifuged at 10,000 rpm for 20 min at 24°C. After centrifugation the melanin was resuspended with a fresh solution of 0.15 EDTA-Na_2 as above and allowed to react for 12 h. The sample was centrifuged and the precipitate washed twice with 10 ml of water. Finally it was washed with acetone and dried under flowing nitrogen gas at 30°C. The yield was 55% of the starting amount of dopamine. The sulfur content was 3.01%

Auto-oxidation procedure

150 mg of dopamine and 15.9 mg of cysteine (molar ratio 7.5:1) were dissolved in a 79 ml volume of 0.050 M phosphate buffer (pH 7.4) solution. The solution was allowed to auto-oxidize in air at 37°C for 4 days protected from light. The suspension was then transferred into glass centrifuge tubes and centrifuged at 10,000 rpm for 15 min. The precipitated melanin was resuspended in 79 ml of a fresh phosphate buffer (0.05 M, pH 7.4) with 15.9 mg of cysteine for 24 h. The treatment was repeated one more time. Finally, melanin was collected by centrifugation as above and suspended in 25 ml of 1% acetic acid, centrifuged, and washed with 25 ml of water. Then is was reacted twice with 0.15 M of EDTA-Na_2 and washed with water and acetone as described for the enzymatic procedure. After drying the yield was 28% with respect to the initial amount of dopamine. The sulfur content was 3.17%.

Binding of Fe(III) to synthetic melanins

In order to add iron to the synthetic samples they were suspended in 1 ml of citrate buffer (1 M, pH 7.4) by sonicating for 30 min. The pigment was allowed to rehydrate under shaking overnight. The melanin suspension was mixed with a ferric citrate solution (180 μl of Fe(III) 70 μmol/ml in sodium citrate, 1 M, pH 7.4) according to a w/w ratio of 1/1.5 of melanin to iron and this solution was kept at room temperature for 48 h, under shaking and in the dark. Then the synthetic melanin was collected by centrifugation, and washed with the previously described citrate buffer

solution twice in order to eliminate the unbound iron. The sample was finally washed twice with water, dialyzed as described before for natural NM, and dried under vacuum. These samples had sufficient iron content so that they were readily analyzable with XAFS techniques. The iron content measured by total reflection x-ray fluorescence was 15.4 μg/mg in the synthetic NM obtained enzymatically and 11.5 μg/mg in the synthetic NM prepared by auto-oxidation.

Description of XAFS measurements

XAFS is a technique which is used to probe the near-neighbor environment of a particular atomic species in a material by measuring the x-ray absorption of a sample, scanning the energy of an x-ray beam through an inner shell absorption edge of the atom of interest from about 200 eV below the edge up to 1000 eV above the edge. Above the absorption edge, the incident x-ray photon ejects an inner shell electron whose energy is given by the difference between the incident and absorption edge energies. This photoelectron then propagates outward and scatters off of neighboring atomic potentials. The interference of the outgoing photoelectron wave and the reflected wave (at the site of the absorbing atom) modulates the absorption coefficient, observed as oscillations in the absorption spectrum above the edge as shown in Fig. 1.

A commonly presented form of the theoretical expression which describes XAFS, $\chi(k)$, the normalized oscillations in the absorption above an absorption edge, is

$$\chi(k) = \sum_j \frac{N_j}{kR_j^2} S_0^2(k) F_j(k) e^{-2k^2\sigma_j^2} e^{-2k/\lambda} \sin[2kR_j + \delta_j(k)], \quad (1)$$

where k is the electron wave number related to the energy, E, of the incident x-rays and E_0 is the energy of the absorption edge for the atom being probed, and it is given by

$$k = \left[\frac{2m_e}{\hbar^2}(E - E_0)\right]^{1/2}. \quad (2)$$

Eq. 1 is described in more detail elsewhere (Stern, 1988); however, the primary features of the equation are as follows. $\chi(k)$ is proportional to N_j, the number of atoms of a particular type at a distance, R_j. The amplitude envelope, $F_j(k)$, is element dependent and can in many cases be used to determine the near neighbor species. Finally, the oscillatory sine term shows how the frequency of the fine-structure oscillations increases with the separation of the absorbing and neighboring atoms. These oscillations are modified by a phase shift, $\delta_j(k)$, which depends on the absorbing atom and the type of neighboring atom, j. The first exponential term reflects a damping of the XAFS oscillations by thermal and structural disorder, with the variable, σ_j^2, a Debye-Waller factor-like term, which is a measure of the mean-square variation of the distance between the scattering atom and its neighbors of type j.

This particular expression for $\chi(k)$ takes into account the random orientation of the structural units in these melanin powder samples. However, samples with a preferred orientation would have some dependence on the orientation of the sample with respect to the incident x-ray beam polarization. It should be noted that no melanin samples have ever been crystallized, and their diffraction patterns resemble those of an amorphous material (Cheng et al., 1994). This form of the equation does not describe multiple scattering. However, some of the results discussed below are, in fact, based on a multiple-scattering formalism for XAFS.

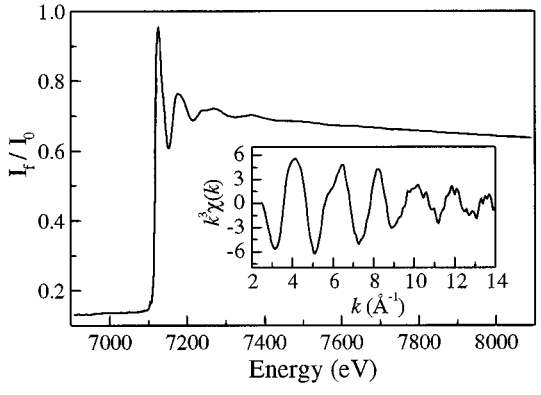

FIGURE 1 A typical fluorescence Fe K-edge XAFS scan for the synthetic melanin sample. Background subtracted k^3-weighted $\chi(k)$ data (*inset*).

Experimental details

The XAFS measurements were performed on the X23-A2 and the X11-A beam lines at the National Synchrotron Light Source at Brookhaven National Laboratory with the storage ring operating at an electron energy of 2.584 GeV and a maximum stored current of 360 mA. Data were collected at X23-A2 using a monochromator with a pair of Si(311) crystals and a beam slit of approximately 1.5 mm high by 1.5 mm wide at the sample, while data collected at X11-A were taken using a monochromator with a pair of Si(111) crystals and a beam slit size of 1.0 mm high by 1.5 mm wide. Near edge spectra were obtained on the X23-A2 beam line with a resolution of ~1.0 eV as determined from beam line measurements, crystal reflection indices, and beam divergence according to Bianconi (1988). XAFS spectra were collected in both transmission and fluorescence detection modes simultaneously as a cross-check on the XAFS amplitudes. Because the samples had an iron mass concentration of 0.3–1.3%, as calculated from the measured transmission edge step and sample density, and were embedded in a low-Z matrix, no x-ray filter was used in the fluorescence measurements. The photon flux incident upon the samples was ~10^9 photons/s, and the detected photon flux above the absorption edge was ~5×10^5 photons/s in the fluorescence mode. Nonetheless, in all cases, the fluorescence measurements were superior to the transmission measurements in the signal/background because of the thin sample(s) and low iron concentration.

The incident intensity (I_O), transmission (I_T), and fluorescence (I_F) detectors were ionization chambers. Both I_O and I_T were of the long, narrow gap design while I_F was a larger area detector. The I_O chamber was filled with a 50:50 mixture of He and N gases, while the I_T chamber at X23A2 was filled with pure nitrogen and at X11A was filled with a 80:20 mixture of N/Ar. The I_F detectors at both lines were filled with Ar gas. Harmonic rejection was accomplished at X11A by detuning to 50% of the maximum intensity. Since fluorescence measurements were the primary mode, no additional harmonic rejection was used at X23A2 other than relying on the insensitivity of the I_O detector to the higher energy x-rays and the much-reduced photon flux at the higher energies. At the expected level of harmonic contamination any effect of the remaining harmonic content should be limited to a slightly higher noise and a slightly higher background, which is eliminated in the later data processing.

XAFS data and analysis

The data were analyzed using a locally-modified version of the UW/NRL XAFS analysis package. This procedure is discussed in detail elsewhere (Sayers and Bunker, 1988). After removing the slowly varying background above the edge using a cubic spline function (in most cases, four sections were sufficient), the XAFS data, normalized to the edge step, were mapped from x-ray energy space to electron wave number space (k-space). A typical fluorescence scan and the normalized XAFS, $\chi(k)$, are shown in Fig. 1. The fluorescence XAFS amplitudes for the first shell were compared to the transmission amplitudes and were found to need correction for self-absorption. This correction is well known for fluorescence detection; here, we use the method of Tan et al. (1989) to accomplish this correction.

The calculated and experimentally determined corrections were consistent with each other; in all cases the necessary amplitude correction was $<10\%$.

Because of the low-Z backscatterers in melanin, a k^3 weighting of the $\chi(k)$ data was necessary in the background removal and following analysis. The Fourier transforms into "r-space" (a radial distribution function except for a phase-shift correction) were performed using a modified Hanning window function generally set between 3.00–11.45 $Å^{-1}$ and rolled off over 0.5 $Å^{-1}$ outside of that range. Various other window parameters and k-weightings were used to check the consistency of the data.

Transmission data of several iron oxide powder samples were used as experimental "standards" for calibrating the theoretical backscattering amplitudes generated by the widely accepted theoretical code FEFF version 6.01 (Rehr et al., 1991). The suitability of FEFF for this study was verified by comparison with experimental data from iron oxides (particularly FeO); this detailed comparison was useful for determining both experimental and theoretical uncertainties. With the exception of automatically maximally overlapping the atomic potentials, the default input parameters were used in the FEFF calculations. The Hedin-Lundqvist self-energy was used to calculated the atomic potentials. Different values for the ionization state of the absorbing Fe atoms were tried, but made only a small change to the calculated XAFS. Since negative and non-integer ionization values were not allowed by FEFF, the entire structure could not be ionized consistently.

RESULTS AND DISCUSSION

The Fourier-transformed XAFS data in Fig. 2 show a clear difference between the $\tilde{\chi}(r)$ for synthetic and natural NMs. While the reverse transform of the isolated first shell in Fig. 3 shows that the nearest-neighbor atoms are essentially the same, the difference in the higher shells is a clear fingerprint that distinguishes the sample as either synthetic or natural. All synthetic samples examined so far have shown a second-nearest-neighbor peak at about 2.25 Å interfering with the first shell. The two natural samples each have well separated first and second coordination shells and are very similar to each other. The double second-shell peaks in $\tilde{\chi}(r)$ for the natural samples are located at 2.7 and 3.15 Å, while the peak at about 2.2 Å arises from the extended structure of the nearest-neighbor atoms.

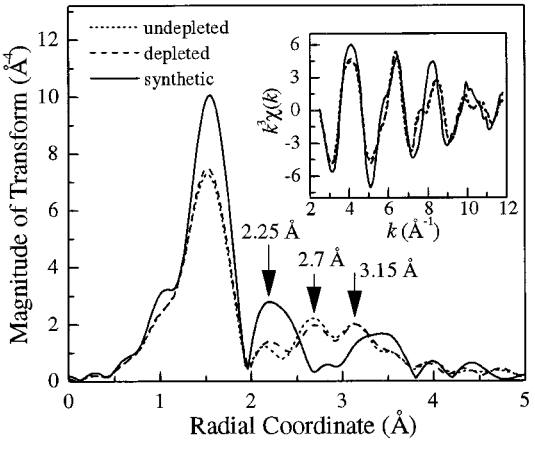

FIGURE 2 Magnitude of the Fourier transform, $\chi(r)$, as a function of the radial coordinate. The second shell peaks are designated by *arrows*. Fourier transform is over a k-space range of 3.5–11.25 $Å^{-1}$ with a modified Hanning window function rolled off over 0.5 $Å^{-1}$. The data shown are for the three NM samples studied. $\chi(k)$ data (*inset*).

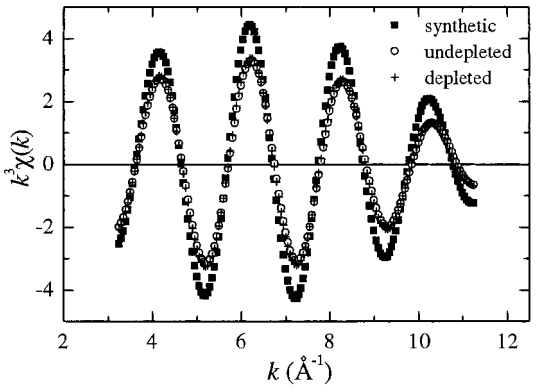

FIGURE 3 Inverse Fourier transform of filtered first shell data for the three samples. r-Space range 1.15–1.90 Å, dr = 0.2 Å.

The XAFS data were fit using *feffit* (Stern et al., 1995), a computer program which takes theoretical scattering paths from FEFF and performs a nonlinear least-squares fit to the data from user-defined variables. A full analysis of the errors and correlation between the variables is performed. The criterion used to determine the error bars for each variable was to find the value that would increase the (statistical) χ^2 value by one as well as investigating the best-fit values for different averaged subsets of the raw data. This χ^2 parameter was scaled by the amplitude of the high-frequency noise in the Fourier-transformed data.

It is known from the sample composition that possible first shell constituents are C, N, O, S, and Fe. Interpretation of the data depends on assumptions of the coordination chemistry. Iron is easily eliminated since the near neighbor atomic spacing is far too close to accommodate Fe-Fe neighbors. Similarly, our results show that the first coordination shell cannot be composed of sulfur atoms, as the phase of the sulfur scattering path is out of phase with the experimental XAFS data for reasonable near neighbor distances based on the atom's covalent radius. In addition the sulfur content is far too small to account for the data. On the other hand, since C, N, and O are next to each other on the periodic table they are very difficult to distinguish from each other as near neighbor atoms. Despite this, carbon is highly unlikely, both from the fit results and the known chemistry. While our data are fit slightly better assuming N rather than O nearest neighbors, the resulting coordination number for nitrogen is an unlikely 8 ± 1, given the nitrogen concentration in the samples. Coordination numbers for oxygen range from 5.8 to 6.6 for the different samples.

Although theoretical scattering paths are increasingly used and considerably more accurate than in the past, fitting to a known experimental standard is still desirable, when possible, to eliminate systematic error in the measurement. This was attempted using iron oxide data, but due to the overlap of the first oxygen and iron shells about the iron atom, it is not possible to satisfactorily separate them to perform a direct experimental comparison. The clearest of the iron oxide standards, FeO, was well fit over the first two

shells using theoretical backscattering amplitudes assuming a large asymmetry in the first shell oxygen distance distribution. This provided a good calibration point to set externally the S_0^2 value in Eq. 1 for the melanin samples. The S_0^2 value determined from the iron oxide standards is 0.79 ± 0.04.

Although very good results are obtained assuming only one neighboring element, if one considers only the extended XAFS, it remains a possibility that the first shell is a mixture of atoms since the C, N, and O backscattering amplitudes and phases are so similar. The possibility of a mixed first shell is discussed further with respect to the near-edge structure.

In Table 1, the results of fitting the first coordination shell to theoretical backscattering amplitudes are tabulated. The nearest-neighbor oxygen distance is 2.00 Å for the synthetic NM and 1.98 Å for the natural NMs. The Debye-Waller factor is a measure of the distribution of atoms around this best fit distance. The natural samples exhibit a larger disorder. Because the first shell constituents are the same for the natural and synthetic samples, the thermal components should be similar. The increase may thus be attributed to a larger structural disorder.

Other methods for single shell analysis, including the ratio method (Sayers and Bunker, 1988), proved less reliable in obtaining consistent values under different conditions. This is due to the interference of the first and second shells in the synthetic samples. Since it is not possible to completely isolate the nearest-neighbor contribution, one must consider at least the next-nearest neighbors in an effort to obtain the most accurate results.

The absorption cross-section near the onset of the absorption edge (both below and above) is shown in Fig. 4*a*. Of particular interest is a feature at energies below the absorption edge itself. A close look at this pre-edge peak reveals a slightly larger peak for the natural samples. It is well known that this pre-edge feature at the Fe K-edge is due to a 1s→3d transition that would be excluded by dipole selection rules for a high-symmetry site (Bianconi, 1988). The observed pre-edge peak in the raw data here indicates a breaking of the inversion symmetry around the Fe site. By comparison of the size of the pre-edge peak, normalized to the step height, with iron oxide reference data (Fig. 4 *b*) it is determined that the first shell is structurally distorted from inversion symmetry. For FeO, with an asymmetric first shell

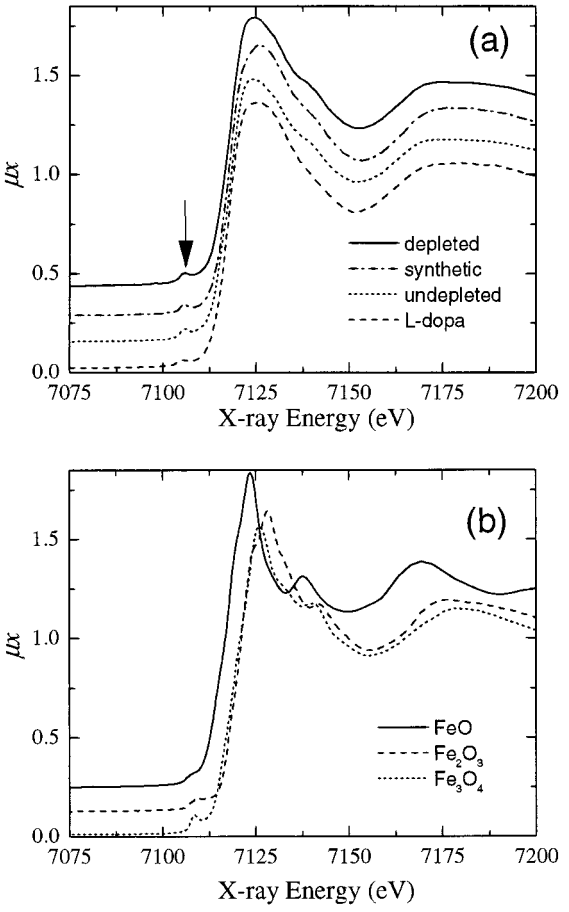

FIGURE 4 (*a*) Near-edge structure of melanin data showing the pre-edge peak, designated by the *arrow*. (*b*) Pre-edge peak normalized to the step height with iron oxide reference data.

distribution, the pre-edge peak is merely a shoulder at the base of the edge, primarily due to the proximity of the peak and edge positions. For Fe_3O_4, which has two distinct near-neighbor oxygen distances, the pre-edge peak is nearly twice as large as for the melanin samples. The pre-edge peak of the melanin samples most closely resembles that of Fe_2O_3 in size and Fe_3O_4 in character suggesting that the first coordination shell is indeed composed of only one type of atom in a structurally distorted arrangement with a well-defined bond length. Fe_2O_3 and Fe_3O_4, being ferric as opposed to ferrous have an edge position shifted to higher energy, separating the edge from the pre-edge peak. The NM samples also show this feature, pointing to the ferric nature of the Fe site. Since a mixed first shell would involve greater breaking of the inversion symmetry, the transition probability from the 1s to the 3d state would likely increase, resulting in a pre-edge feature which would likely be either more pronounced or exhibit more fine structure than do the melanin samples.

Fitting the second and higher shells poses a similar problem as solving a mixed first shell. In the case of the synthetic NM, there are distinct second and third nearest-neighbor peaks. Although the second shell can be fit rea-

TABLE 1 Fluorescence-corrected first shell XAFS coordination numbers, radial distances, and Debye-Waller factors for melanin samples

Sample	Coordination number	Radial distance (Å)	XAFS DW factor ($\times 10^{-3}$ Å^2)
Synthetic	6.6 ± 0.5	2.00 ± 0.02	6.3 ± 0.8
Depleted natural	6.0 ± 0.6	1.98 ± 0.02	9.0 ± 1.2
Undepleted natural	5.8 ± 0.6	1.98 ± 0.02	9.0 ± 1.2

Samples obtained by fitting the room temperature XAFS data to a theoretical model of the amplitude and phase.

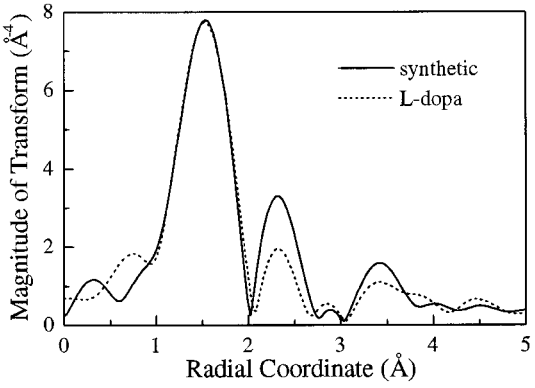

FIGURE 5 Fourier transform magnitude as a function of the radial coordinate for the synthetic NM and L-dopa. Fourier transform over k-space range of 3.25–8.75 Å^{-1} with a modified Hanning window function rolled off over 0.5 Å^{-1}. Data are normalized to have a nearly equivalent first-shell amplitude for clarity.

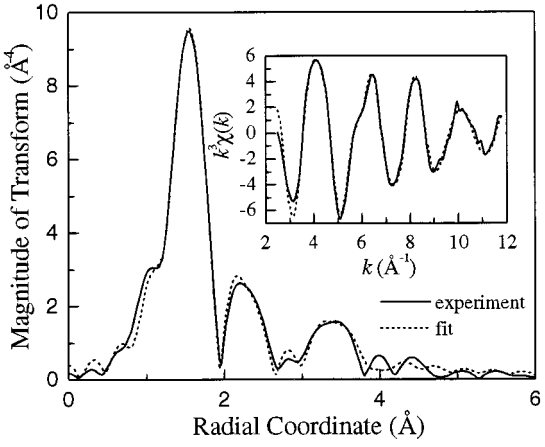

FIGURE 7 Fit of the synthetic melanin structure in r-space using theoretical XAFS amplitudes. The inverse Fourier transform over the first three shells is shown in *inset* (*open circles*) with the fit results (*solid line*).

sonably well with one scattering path, since the higher shells all clearly interfere in r-space, they must be treated together instead of individually. XAFS data were collected on a sample of L-dopa melanin and the Fourier transform is plotted in Fig. 5 along with the synthetic NM data. Since the data are similar, the presumed Fe site in L-dopa might serve as a model for the Fe site in the synthetic NM. The proposed structure is an iron atom coordinated to two pairs of oxygen atoms that are part of two quinone-like structures (Fig. 6). Since the first-shell coordination number is six, there must also be two oxygen atoms, perhaps from hydration of the sample, out of the plane determined by the two quinone-like structures. This model for the near-neighbor environment of Fe fits the synthetic melanin XAFS data very well out to the third-nearest neighbor (~4.0 Å) as shown in Fig. 7.

Examining the proposed structure in Fig. 6, one can see a nearly collinear arrangement between the Fe-O-C2 and the Fe-C1-C2 sets of atoms, where C1 and C2 refer to the carbon atoms nearest to and second nearest to the iron atom, respectively. This suggests that there will be strong multiple-scattering contributions to the XAFS. Including these multiple-scattering paths is found to significantly improve the fit quality. Indeed, the third peak in the $\tilde{\chi}(r)$ spectrum, is nearly entirely due to multiple scattering paths; Fe-Cl-C2, Fe-C1-C2-C1, Fe-O-Fe-O and Fe-O-C1. The parameters varied in the fit procedure include the radial distance of paths (Fe-O, Fe-C1, Fe-C2, Fe-C1-C2), the amplitudes of the Fe-O and Fe-C1 paths, the Debye-Waller factor of each of the three single scattering paths, and the E_0 energy offset; a total of ten independent variables. All other parameters were tied to these independent variables. Note that the contributions of these multiple-scattering paths to the XAFS are extremely sensitive to the precise geometry of the material and although this is by no means the only model which could fit the data, because of the sensitivity of the XAFS to multiple scattering contributions, this model is a good candidate.

The available data range for the synthetic sample is larger than for the natural samples due to several glitches in the spectra above 12 Å^{-1}. For consistency in reporting, the same data ranges were used for the analysis of all samples. Extending the fitting range for the synthetic NM data up to 14.5 Å^{-1} did not significantly alter the values presented in Table 2, although the third-nearest neighbor fit does begin to degrade at larger transform ranges compared to the smaller Fourier-transform range.

The diffraction analysis of L-dopa (Cheng et al., 1994) has led to a model structure for a protomolecule consisting

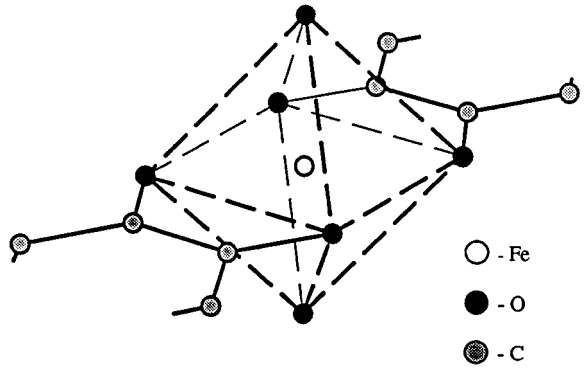

FIGURE 6 Model of the synthetic melanin structure used for the theoretical model of the XAFS data.

TABLE 2 Full fit results for synthetic melanin model applied to synthetic melanin XAFS

Path	Coordination number	Radial distance (Å)	XAFS D-W factor ($\times 10^{-3}$ Å^2)
Fe-O	6.6 ± 0.5	2.00 ± 0.02	6.3 ± 0.8
Fe-C1	5.9 ± 2.2	2.82 ± 0.02	8.0 ± 3.5
Fe-C2	5.9 ± 2.2	4.13 ± 0.03	9.0 ± 8.0

k^3 weighting, k-space range 3.0–11.45 Å^{-1}, dk = 0.5 Å^{-1}, r-space range 1.15–3.9 Å. Fit results for the multiple scattering paths are consistent with the near neighbor distances above when arranged as in Fig. 5.

of four imperfectly stacked planar sheets, each sheet containing eight 5,6-indolequinone molecules, linked together so that the oxygens lie on the outer edge of each sheet and the nitrogens located in a porphyrin-like hole in the center of the sheet. In this model the iron would lie between a pair of planar sheets contained in the different melanin protomolecules. Assuming similar sizes and composition for neuromelanins, at the concentration of Fe present in the measured samples there is of the order of one Fe atom per protomolecule. In addition to the two pairs of "quinone-like" oxygens provided by the planar sheets forming the iron complex, the additional two oxygens required for six-fold coordination, would most likely be in the form of OH radicals or perhaps even water molecules. It should be noted that the state of binding of the oxygen atoms in the coordination sphere cannot readily be identified with XAFS, so that the oxygens might be singly or doubly bonded, charged or uncharged or bound to an H atom, which would be essentially invisible to XAFS.

In the natural samples, the larger distance peak is a broad peak, well separated from the first shell. All attempts to fit this higher shell structure with a model similar to the synthetic NM have met with failure. The second shell peak is located farther away from the first shell peak for the natural samples than for the synthetic samples and therefore cannot have a radial distance consistent with the model. Although the octahedral oxygen nearest neighbor structure is still valid the bonding of the oxygens to the remaining melanin structure must be significantly different.

The double peak in the second shell of the natural samples indicates two scattering paths of nearly the same distance. In the high-energy portion of the spectrum, the XAFS of the two sub-shells interfere constructively and look like just one shell. When a larger data range is transformed, in this case to lower energy values, the XAFS of the two sub-shells begin to destructively interfere causing the additional structure to appear in the second shell. Since the sub-shells are in phase over a fairly wide range (at least 5 $Å^{-1}$) the atoms composing the shells are near to each other on the periodic table; either the same element or a combination of C, N, or O. The distances to the two sub-shells are 3.45 ± 0.05 Å and 3.78 ± 0.05 Å respectively. The possibility that the second-shell interference in the XAFS is caused by multiple scattering was investigated. However, the scattering angle for the multiple-scattering path would be less than 140° while multiple scattering amplitudes begin to drop off rapidly as angles decrease below 150°.

The presence of two distinct binding sites for iron in synthetic dopamine-melanin was previously described (Ben-Shachar et al., 1991); however, its structure is quite different from that of natural NM (Zecca et al., 1992, 1996). Since the Fe concentration in the depleted natural sample is ~30% of that in the undepleted sample, from the XAFS data (Fig. 2), after correcting for self-absorption, it is apparent that the natural melanin samples are virtually identical before and after depletion. The differences in the first-shell structural parameters are within experimental error. The second and higher shells are also the same given experimental error and sample to sample variation. Although Fe may occupy several nonequivalent sites in natural NM, Fe is depleted equally from all these sites. This makes it likely that the sites are not distinguished by their ability to hold Fe atoms, but rather by the location of the sites in the melanin particle. Fe from surface sites and near surface sites would diffuse more rapidly and be removed at a faster rate than Fe from deep interior sites. Dynamics of melanin aggregation (Huang et al., 1989) show melanin to have a fractal structure implying a sponge-like structure with enhanced surface and near surface sites. Such structures would slow depletion of iron from the interior sites.

Preliminary low temperature XAFS measurements were also performed at 80 K and 25 K and will be discussed in a future paper. These results nonetheless illuminate the near-neighbor environment of Fe in the melanin samples. For the natural samples, the decreasing temperature change and associated decrease of the thermal component of the Debye-Waller factor corroborate the absence of nearest-neighbor Fe atoms whose presence would be evidenced by an increasingly large second-shell peak relative to the first shell peak on cooling.

This telltale sign does appear, to a small degree, in the synthetic melanin samples. While the presence of a small number of nearby Fe atoms (less than two) is consistent with the XAFS, the addition of second-shell Fe does not necessarily contradict the model previously proposed for the synthetic melanin. For the best results, a number of C atoms remain in the second shell, although the Fe-C distance expands to 2.89 ± 0.04 Å. The evidence for next-nearest neighbor Fe atoms is merely suggestive, not conclusive. Our statistically more reliable results are therefore as presented, without nearby Fe atoms. Nevertheless, a more in-depth study of the temperature dependence of the XAFS is necessary in order to settle this question.

The XAFS results show no evidence of close iron neighbors in the natural NM, which in turn makes it unlikely that the natural NM is superparamagnetic, contrary to the interpretation offered by the Mössbauer studies. Our preliminary magnetic susceptibility measurements made on natural NM show only paramagnetic behavior. The hyperfine splitting observed at low temperatures in Mössbauer studies requires only that the relaxation time for reordering the atomic magnetic moment be comparable to the relaxation time for reorienting the nuclear moment of Fe. It is clear that the Fe in NM does not follow the ferritin model.

CONCLUSIONS

The Fe XAFS signal for NM SN melanins, synthetic NMs, and L-dopa melanin show the pre-edge feature associated with a dipole forbidden $1s \rightarrow 3d$ transition indicative of a breaking of inversion symmetry around the Fe site. Comparison of the pre-edge peak with those associated with known standards leads to the conclusion that the first coor-

dination shell is composed of six oxygens in a structurally distorted octahedral arrangement with a Fe-O bond length of 1.99 ± 0.02 Å. Analysis of the isolated first shell data for all samples leads to this conclusion. We should, however, emphasize that the Fe-O distances are nonetheless slightly different in the synthetic and natural samples (Table 1).

Distinct differences between the synthetic and natural samples are apparent in the features arising from the next nearest neighbors. All synthetic NMs, as well as L-dopa, show a single second nearest neighbor peak interfering with the first shell, while both the depleted and undepleted NM SN samples each have well separated first and second coordination shells.

No difference was observed between the XAFS signals for the undepleted and depleted NM SN samples. Although the Fe content was reduced to about one-third in the depletion process, there is no evidence to indicate that the depleted Fe occupied a distinctly different site.

Analysis of the XAFS data from both synthetic NMs and L-dopa, taking into account multiple scattering effects, has led to the development of a model which has produced a good fit to the experimental data. A more detailed knowledge of the NM structure and NM-Fe complex is necessary to understand the role of this pigment in brain aging and Parkinson's disease.

We thank Grant Bunker for the use of iron oxide data, which we used to verify our analysis, as well as for useful advice pertaining to Fe K-edge XAFS of proteins. We thank Pei Hor for magnetic susceptibility measurements and Richard Frankel for useful discussions.

The X23-A2 beam line is supported in part by the National Institute of Standards and Technology. We gratefully acknowledge the support of the U.S. Department of Energy, Division of Materials Science, under Contract DE-FG05–89ER45384 for its role in the development and operation of beam line X11 at the National Synchrotron Light Source. At Houston this work has been supported by the U.S. Department of Energy, Division of Materials Science on Contract DE-FG05–87-ER45325. In Milan this work was supported by the Italian Association for Parkinson's Disease. The National Synchrotron Light Source is supported by the Department of Energy, Division of Materials Science and Division of Chemical Sciences under Contract DE-AC02–76CH000016.

REFERENCES

Bardani, L., M. G. Bridelli, M. Carbucicchio, and P. R. Crippa. 1982. *Biochim. Biophys. Acta.* 716:8–15.

Ben-Shachar, D., and M. B. H. Youdim. 1993. *Prog. Neuro-Psychopharmacol. Biol. Psychiat.* 17:139–150.

Ben Shachar, D., P. Riederer, and M. B. H. Youdim. 1991. *J. Neurochem.* 57:1604–1609.

Bianconi, A. 1988. XANES spectroscopy. *In* X-Ray Absorption: Principles, Applications, Techniques of EXAFS, SEXAFS, and XANES, edited by D. C. Koningsberger and R. Prins. Wiley, New York.

Cheng, J., S. C. Moss, and M. Eisner. 1994. *Pig. Cell Res.* 7:263–273.

Gerlach, M., A. X. Trautwein, L. Zecca, M. B. H. Youdim, and P. Riederer. 1995. *J. Neurochem.* 65:923–926.

Gibb, W. R. G. 1992. *Brain Res.* 581:283–291.

Hirsch, E. G., A. M. Graybiel, and Y. Agid. 1988. *Nature.* 334:345–348.

Huang, J. S., J. Sung, M. Eisner, S. C. Moss, and J. Gallas. 1989. *J. Chem. Phys.* 90:25–29.

Jellinger, K., E. Kienzl, G. Rumpelmair, P. Riederer, H. Stachelberger, D. Ben-Shachar, and M. B. H. Youdim. 1992. *J. Neurochem.* 59: 1168–1171.

Rehr, J. J., J. Mustre DeLeon, and S. I. Zabinsky. 1991. *J. Am. Chem. Soc.* 113:5135.

Sayers, D., and B. Bunker. 1988. Data analysis. *In* X-Ray Absorption: Principles, Applications, Techniques of EXAFS, SEXAFS, and XANES, edited by D. C. Koningsberger and R. Prins. Wiley, New York.

Shima T., T. Sarna, A. Stroppolo, R. Gerbasi, H. M. Swartz, and L. Zecca. 1997. *Free Rad. Biol. Med.* 23:110–119.

Stern, E. 1988. Theory of EXAFS. *In* X-Ray Absorption: Principles, Applications, Techniques of EXAFS, SEXAFS, and XANES, edited by D. C. Koningsberger and R. Prins. Wiley, New York.

Stern, E., M. Newville, B. Ravel, Y. Yacoby, and D. Haskel. 1995. *Physica B.* 208,209:117.

Swartz H. M., T. Sarna, and L. Zecca. 1992. *Ann. Neurol.* 32:S69–S75.

Tan, Z., J. I. Budnick, and S. Heald. 1989. *Rev. Sci. Instruments.* 60: 1021–1025.

Zecca L., C. Mecacci, R. Seraglia, and E. Parati. 1992. *Biochim. Biophys. Acta.* 1138:6–10.

Zecca L., R. Pietra, C. Goj, C. Mecacci, D. Radice, and E. Sabbioni. 1994. *J. Neurochem.* 62:1097–1101.

Zecca, L., T. Shima, A. Stroppolo, C. Goj, A. Battiston, R. Gerbasi, T. Sarna, and H. M. Swartz. 1996. *Neuroscience.* 73:407–415.